ANNUAL REVIEWS

Annual Review of Biomedical Engineering

Electrophysiological Source Imaging: A Noninvasive Window to Brain Dynamics

Bin He,[1,2] Abbas Sohrabpour,[2] Emery Brown,[3] and Zhongming Liu[4]

[1]Department of Biomedical Engineering, Carnegie Mellon University, Pittsburgh, Pennsylvania 15213, USA; email: bhe1@andrew.cmu.edu

[2]Department of Biomedical Engineering, University of Minnesota, Minneapolis, Minnesota 55455, USA

[3]Institute for Medical Engineering and Science, Massachusetts Institute of Technology, Cambridge, Massachusetts 02139, USA

[4]Weldon School of Biomedical Engineering, School of Electrical and Computer Engineering, and Purdue Institute of Integrative Neuroscience, Purdue University, West Lafayette, Indiana 47906, USA

Annu. Rev. Biomed. Eng. 2018. 20:171–96

First published as a Review in Advance on March 1, 2018

The *Annual Review of Biomedical Engineering* is online at bioeng.annualreviews.org

https://doi.org/10.1146/annurev-bioeng-062117-120853

Keywords

electrophysiological source imaging, EEG, MEG, source localization, functional connectivity, inverse problem

Abstract

Brain activity and connectivity are distributed in the three-dimensional space and evolve in time. It is important to image brain dynamics with high spatial and temporal resolution. Electroencephalography (EEG) and magnetoencephalography (MEG) are noninvasive measurements associated with complex neural activations and interactions that encode brain functions. Electrophysiological source imaging estimates the underlying brain electrical sources from EEG and MEG measurements. It offers increasingly improved spatial resolution and intrinsically high temporal resolution for imaging large-scale brain activity and connectivity on a wide range of timescales. Integration of electrophysiological source imaging and functional magnetic resonance imaging could further enhance spatiotemporal resolution and specificity to an extent that is not attainable with either technique alone. We review methodological developments in electrophysiological source imaging over the past three decades and envision its future advancement into a powerful functional neuroimaging technology for basic and clinical neuroscience applications.

Contents

1. INTRODUCTION

The human brain comprises roughly 100 billion neurons (1). Each of these building blocks of the brain forms an average of 10^3–10^4 synapses, creating a huge network with quadrillions of connections that enables our brains to function as they do (2). Although a great deal is known about neurons on the microscopic scale, little is known about how these huge numbers of neurons (and synapses) work collectively to give rise to macroscopic brain signals and human behaviors.

Human brain functions are carried out by complex neural activations and interactions, which elevate electromagnetic signal changes (primary effects) accompanied by hemodynamic and metabolic changes (secondary effects). These changes represent the basic sources for all noninvasive neuroimaging techniques. Depending on the signal sources, these imaging techniques can be divided into two categories. The first category involves direct imaging of neural electrical sources by detecting the induced electromagnetic signal changes by use of electric or magnetic sensors over the scalp. Common methods in this category are electroencephalography (EEG) and magnetoencephalography (MEG). The second category consists of indirect imaging approaches based on hemodynamic (cerebral blood flow, cerebral blood volume) and/or metabolic (glucose and oxygen utilization) changes associated with neural activity. Common methods in this category are functional magnetic resonance imaging (fMRI), positron emission tomography (PET), single-photon emission computed tomography (SPECT), and near-infrared spectroscopy.

Brain activation is accompanied by induced electrical activity due to excitation of neurons. The electrical activity of the brain can be analyzed on a variety of scales, depending on the study's aim and focus, including levels of ion channels, synapses, neurons, neuronal ensembles, lamina,

columns, regions, and networks. Invasive electrophysiological recordings, such as spike trains and local field potentials (LFPs), as well as intracranial EEG, have contributed to our understanding of neuronal activities at the microscopic or mesoscopic scale. Understanding human brain dynamics at the macroscopic scale, however, relies on noninvasive measurement techniques such as EEG and MEG (3, 4). Importantly, activation of single or multiple neurons does not lead to detectable EEG/MEG signals; instead, it requires the synchronous excitation of a large number of neurons to generate detectable signals. Thus, EEG/MEG report rich information about brain function (or dysfunction) encoded by dynamics of large-scale brain networks, making EEG and MEG studies highly relevant for clinical, cognitive, and behavioral brain research.

In EEG/MEG, the measured electrical or magnetic field changes reflect instantaneous neuronal currents, given that electromagnetism in the brain can be treated in a quasi-static condition (5). Among existing neuroimaging modalities, EEG/MEG offer uniquely high temporal resolution but limited spatial resolution. Significant efforts over the past three decades have greatly advanced electrophysiological source imaging on the basis of EEG/MEG, resulting in high temporal and good spatial resolution that places EEG/MEG among the most widely used tools in neuroscience. This article reviews the principles of electrophysiological source imaging (ESI), the state of the art, and remaining challenges.

2. SOURCE IMAGING CONCEPTS

ESI is the process of estimating neural electrical activity underlying noninvasive electromagnetic measurements such as EEG and MEG (4, 6). ESI counters the effect of volume conduction or field propagation on the reconstruction of brain sources from EEG/MEG. Solving this problem will be difficult if it is approached only mathematically. However, investigators have made significant progress in that anatomical and physiological constraints can be utilized in source estimation. In this section, we describe the origins of EEG and MEG in order to lay the neurophysiological foundation of our discussion of EEG/MEG-based functional neuroimaging.

Given an imbalance between the ions inside and outside a neuron, a change occurs in the potential difference between the cell's interior and exterior. When this change exceeds a certain threshold, the cell produces a sharp deflection of the transmembrane potential—the action potential (7). Action potentials propagate through neuronal axons and travel from one physical point to another, allowing neurons to communicate over a variety of spatial scales (3).

Electrical currents are produced by the movement of charges inside, outside, and along the neuronal cells. The electrical and magnetic fields arising from these microscopic currents, when added constructively, can produce observable electrical or magnetic signals at the macroscopic level. The spatial distribution of these currents determines the overall effect at the scalp (3, 7, 8).

The organization of cortical pyramidal cells makes them the type of neurons most readily detectable with EEG/MEG. These cells are spatially aligned in such a way that, when excited in synchrony, they produce detectable effects on the scalp. EEG/MEG signals arise primarily from postsynaptic currents. Currents that drive action potentials are generally negligible on the scale of EEG/MEG (9).

The elongated shape of pyramidal neurons separates the current inflow and outflow by a short distance. In the extracellular space, such currents are viewed as a pair of current sink and source (monopoles), respectively. For far-field techniques like EEG/MEG, such a pair of current monopoles can be represented as a current dipole. Currents in extended cell populations may also be modeled as quadrupoles (10–12). However, dipole models are more widely used than monopole or multipole models, as dipoles can be viewed as a discrete representation of current density and offer clearer physical and physiological interpretation.

Finding the electromagnetic signals on the scalp arising from neuroelectric currents in the brain is referred to as solving the forward problem of EEG/MEG. The electric and magnetic fields are generated by the currents that propagate through brain tissue and produce an effect on scalp sensors. When the average current density in each volumetric or areal element is modeled as a dipole (or, less frequently, a monopole or multipole), the forward problem can be solved with the superposition principle because the head is considered to be a linear system that generates additive effects of neuronal currents.

In the quasi-static condition, the forward problem can be expressed as solving Poisson's equation (5). The solution depends on the tissue conductivity or permeability and the boundary conditions of electromagnetic fields. When the head geometry is modeled as one or multiple spheres with homogeneous conductivity, analytical solutions exist for the forward problem (7). An important development in ESI has been the ability to perform "constrained" source imaging by using anatomical information (13). Such an anatomical constraint can be obtained from structural MRI, which offers soft-tissue contrast to segment the brain, skull, cerebrospinal fluid, and scalp. For realistic-geometry head models, numeric solutions are attainable with either the boundary element method (BEM) by assuming isotropic conductivity (13, 14) or the finite element method (FEM) by assuming anisotropic conductivity (15). In principle, FEM allows for more accurate head modeling than BEM; however, accurate information about tissue conductivity is not readily available. Since brain source imaging was introduced in the late 1980s (13, 14), BEM has been the most widely used method for anatomically constrained ESI with EEG/MEG.

Unlike the deterministic forward problem, the inverse problem (i.e., the estimation of source distribution given scalp measurements) is known to be underdetermined (16). The number of current sources is significantly greater than the number of measurements, despite high-density EEG/MEG. Inferring source distribution from measurements is challenging without the application of a constraint or regularization based on a priori information about the desired source characteristics or physiological assumptions. Regularization also helps stabilize the solution against noise (17).

An important issue in ESI is adequate spatial sampling. Whereas MEG uses ~150 or more channels of recordings, clinical EEG often uses fewer channels (e.g., 19–32 electrodes). Studies indicate that higher spatial sampling helps improve the precision of ESI (18, 19). A recent guideline from the International Federation of Clinical Neurophysiology suggests that at least 64 channels of EEG should be used for ESI (20). **Figure 1** illustrates the relationship between neuronal excitation, volume conduction, and scalp EEG/MEG, as well as the concept of the forward and inverse problems.

3. SOURCE IMAGING ALGORITHMS

The ESI, as an inverse problem, can be solved by minimizing the difference between the measured signals and those generated by source estimates through the head volume conductor model. Depending on the source models adopted, various techniques have been developed to accomplish this goal. This section discusses some of these techniques to illustrate the general strategies for ESI, but it is not intended to be an exhaustive survey.

3.1. Equivalent Current Dipole Models

In one of the earliest approaches for brain source imaging, whole-brain activity is modeled with a limited number of dipoles (13, 21). Many events or tasks, such as epileptiform activity, involve electrical activity at a focal region, which may be modeled by an equivalent current dipole (ECD)

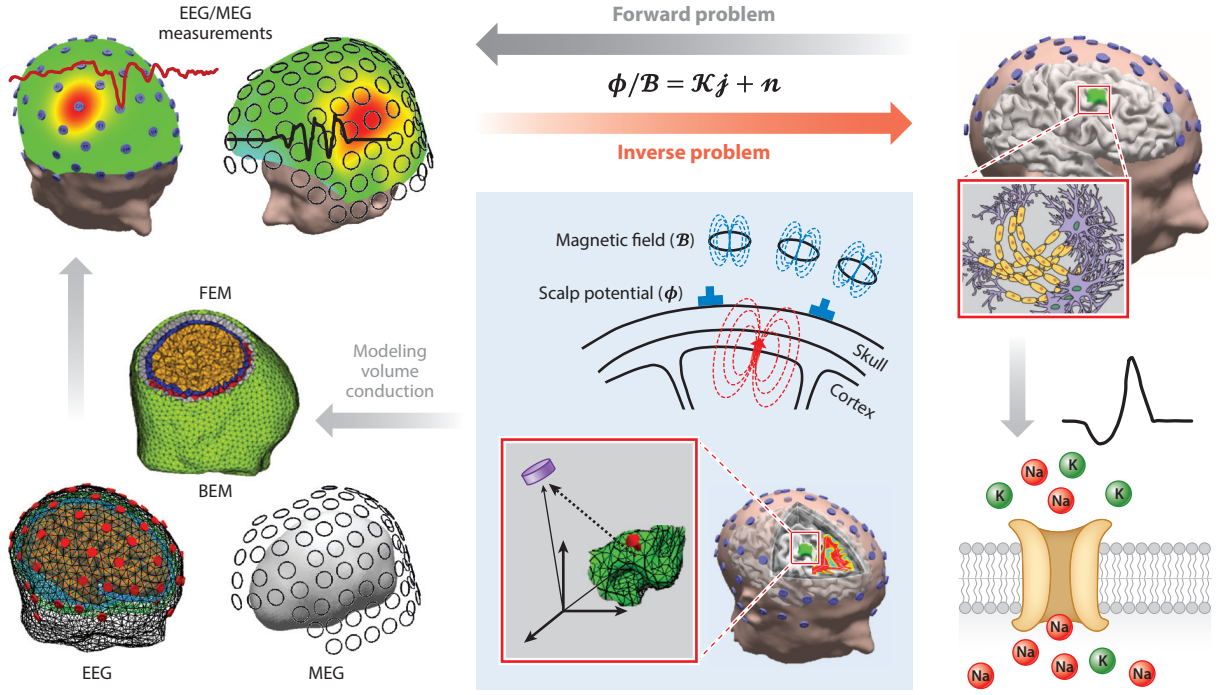

Figure 1

Physiological basis of electroencephalography and magnetoencephalography (EEG/MEG) and the biophysical modeling of the forward and inverse problems. The electrical activity of the brain arises from the ions (charges) that enter and exit the selective membrane of neurons. EEG/MEG signals manifested on the scalp represent the underlying activation of synchronous neuronal ensembles, which encode brain function or dysfunction. Current dipoles can be used to model neuronal currents. Maxwell's equations can be solved to obtain the electric potential (EEG) and the magnetic field (MEG)—the so-called forward problem. Various numerical techniques, such as the boundary element method (BEM) and the finite element method (FEM), can be used to model the head volume conductor linking neuronal current dipoles to EEG/MEG. The current density distribution of brain activity can be estimated from scalp EEG/MEG by means of signal processing algorithms—the so-called inverse problem. The lead-field matrix is denoted by $\mathcal{K}$, the current density distribution as j, and n is the additive noise in the recording EEG/MEG system.

located at the center of this region. Estimating one or two ECDs is an overdetermined inverse problem that has a unique solution, as there are six parameters for each dipole, whereas clinical EEG recordings normally use at least 19 electrodes.

Multiple approaches to dipole source localization exist (22). One is to fit dipoles to scalp recordings separately for each moment; this approach is known as moving dipole localization because both the dipole location and orientation are allowed to vary in time. Another approach is to fix the dipole location but allow the orientation to vary freely, or to fix both the dipole location and orientation but allow only the dipole magnitude to vary. Both approaches are effective in different situations, if (*a*) the number of unknown parameters is smaller than the number of sensors, (*b*) the source activity can be properly modeled as a single dipole or a few dipoles, and (*c*) the number of dipoles is known a priori.

A major challenge for dipole source localization is the nonlinear relationship between EEG/MEG and the dipole locations. When the location of dipole is fixed and known, finding its orientation and amplitude becomes a linear problem (13). For a moving dipole solution, the estimated locations of ECDs provide useful physiological or clinical information.

However, localization of more than two moving dipoles is challenging. The assumption of focal sources is not always valid, and knowing the number of dipoles a priori is not feasible for many applications. The nonlinearity of the moving dipole solution escalates as the number of dipoles increases. These drawbacks limit the scope of application for ECD localization, yet the technique is still being used in clinical neuroscience applications, especially in MEG source localization.

3.2. Distributed Source Models

It is more realistic to describe EEG/MEG sources as a current density distribution, which can be modeled by a large number of current dipoles distributed over the three-dimensional brain volume or two-dimensional cortical surface. The latter is preferable because the sources of EEG/MEG are primarily currents through pyramidal cells aligned perpendicularly to the cortical surface, as proposed by the cortical current density model (23). Because the dipole locations are fixed, the inverse problem of estimating dipole moments from EEG/MEG is linear but underdetermined. A priori information is required to regularize the solutions to this inverse problem. Depending on the physiological plausibility of the regularization introduced, the distributed source estimates bear different characteristics and affinity to neural activity on a mesoscopic scale.

3.2.1. Minimum norm family. The minimum norm (MN) approach was the earliest solution to the bioelectromagnetic inverse problem with distributed source models (24). In this approach, the Euclidean norm (or L_2 norm) of distributed currents is used to regularize the least-squares estimation of the inverse solution. This technique solves the underdetermined inverse problem by choosing a unique source configuration with the minimum energy among all possible solution configurations that equally fit the data. This approach has established characteristics in statistics and mathematics; however, its physiological plausibility is not fully understood despite its wide use in EEG/MEG source imaging.

MN solutions are biased toward superficial sources, as such sources generate stronger fields with less energy due to their spatial proximity to the sensors. One way to mitigate this bias is to weight the current sources by the norm of the EEG/MEG signals that can be generated by each source with a unitary magnitude. Introducing this weighting to MN regularization leads to the so-called weighted minimum norm (WMN) solution (25–28). A variation of WMN is low-resolution electromagnetic tomography (LORETA), in which the norm of the second-order spatial derivative of the current source distribution is minimized to ensure spatial coherence and smoothness (29). Post hoc nonlinear normalization can be applied to the inverse solution obtained by the MN approach or its variations. With the use of this strategy, standardized LORETA (sLORETA) (30) has shown improved spatial accuracy.

The MN approach and its variations have progressively evolved to become some of the most successful ESIs for EEG, MEG, or their combination (31). A main drawback of the MN approach is that the resulting solutions tend to be overly smooth and widespread beyond the extent of the underlying sources.

3.2.2. Beamforming and scanning methods. An alternative method, beamforming, which was originally established for radar and sonar applications (32), is increasingly being used for ESI (33). The central idea is to refocus scalp EEG/MEG signals to their originating locations by spatially filtering EEG/MEG specifically for each source location such that the output of the filter has minimal variance for each source location. As such, this approach is sometimes referred to as linearly constrained minimum variance localization (33, 34). The source estimates can be obtained by applying the optimized filters to the measured EEG/MEG signals. Extensions or variations of

this idea have led to various beamforming approaches (35–37). However, the accuracy of beamforming solutions is of concern when the underlying sources are correlated (37). Beamforming is also sensitive to inaccuracy of the forward model, for example, due to approximation in tissue conductivity. Perhaps for this reason, beamforming is more widely used for MEG than EEG, as the forward problem is relatively simpler for MEG.

A related but distinct technique uses a scanning strategy. That is, all source locations are scanned one by one to quantify how well the scalp map that is forwardly computed from assuming a dipole at each location can be classified as either being in the signal subspace or being in the noise subspace, while the signal and noise subspaces are orthogonal to each other and estimated from EEG or MEG (38, 39). An implementation of this approach is multiple signal classification (MUSIC) (38, 39), in which the nonlinear optimization process of finding the dipole location is avoided. However, MUSIC's performance suffers if the sources to be localized are correlated, especially if they are close to one another (40). Variations of MUSIC, such as recursively applied and projected MUSIC (40) and the first-principles vector localization method (41), mitigate this problem to a certain degree.

3.2.3. Bayesian methods. Bayesian inference provides a general framework in which many source imaging algorithms can be derived and interpreted. Given the Bayes theorem, Bayesian algorithms maximize the posterior distribution of sources given measurements, while assuming a prior probabilistic distribution of the sources. If the prior distributions are not known, noninformative priors (e.g., assigning equal probability to all possible outcomes) may be used, or the prior distribution itself may be marginalized by a set of hyperparameters that can be estimated from data (42). The latter is known as an empirical Bayes method, which successively applies the Bayes rule to iteratively update and jointly estimate the prior and posterior distributions through the technique of expectation maximization (42, 43).

The MN approach and its variations can be viewed as special cases of Bayesian inference algorithms with different prior distributions. For instance, the MN is the maximum a posteriori estimation when the prior distribution is assumed to be a Gaussian distribution (42). More importantly, Bayesian inference allows one to incorporate physiological knowledge in the multivariate prior distribution in order to constrain the locations and connectivity of the unknown sources (44). Bayesian algorithms are more efficient if the prior distribution can be described with fewer hyperparameters, for example, by assuming independent sources (or a diagonal covariance matrix). Selecting and parameterizing the prior distribution are not straightforward tasks, bringing both challenges and opportunities. Bayesian methods have many variants (44–47), such as sparse Bayesian learning algorithms (48), coherent maximum entropy on the mean (49), and dynamic maximum a posteriori expectation–maximization (50), and remain an area of active research.

3.2.4. Sparsity-constrained source reconstruction. Sparsity is often assumed in order to avoid overfitting in inverse problems, and has increasing applications in signal and image processing (44, 51–55). In the context of ESI, the sparsity in the source space means that it has far fewer nonzeros than zeros at specific moments, periods, or frequency bands. The sparsity assumption is not necessarily limited to the spatial domain but may apply to other domains to which the source distribution may be transformed. For instance, sources may be piecewise continuous; although the source distribution is not sparse, its edge or spatial gradient is sparse (56). In general, sources should be described with most compressed (i.e., the least redundant) representations in order to be estimated from limited data—a notion that also underlies compressed sensing (57).

Focal underdetermined system solution (FOCUSS) (51) is an early example of the use of sparsity for ESI. However, the resulting solutions tend to be overly focused. The selective MN method

(58), minimum current estimate (59), and sparse source imaging (52) are other examples of sparse methods in which the sparsity is imposed on distributed current density. L_1-norm regularization favors sparse source distribution (58–61); it assumes that the sources follow a Laplace prior distribution in Bayesian inference. In more recent studies, sparsity is imposed in other domains, such as the gradient domain (56), wavelet coefficients domain (62), and Laplacian domain (53), and even multiple domains combined (55, 63, 64). Recent developments in sparse ESI algorithms suggest the capability of estimating both the source locations and extents (55), reflecting the spatiotemporal characteristics of underlying brain sources and dynamics. **Figure 2** depicts the main classes and families of source imaging algorithms, and illustrates an example of ESI using various algorithms.

4. SOURCE IMAGING APPROACHES AND APPLICATIONS

Neural activity of interest to EEG and MEG includes ongoing activity in the absence of any task, or the responses evoked or induced by various events. Endogenous events such as interictal spikes, seizures, and motor imagination spontaneously emerge during cognitive or pathological processes. Evoked potentials and event-related potentials (ERPs) are related to external stimuli or tasks. Despite the differences among these events, they may be imaged with similar ESI techniques.

4.1. Imaging External Event–Related Brain Activity

External events trigger rapid brain responses. EEG/MEG are uniquely well suited to resolving the full response dynamics due to their high temporal resolution. ESI further enhances the spatial resolution and specificity toward comprehensive spatiotemporal imaging of the brain in action. Applications of ESI have been demonstrated in numerous basic and clinical neuroscience studies. For example, ESI has been used to map the spatiotemporal responses underlying sensory processing, object recognition (65), disrupted visual processing in autistic patients (66), attention and consciousness (67), visual rivalry (68–70), and speech recognition (71). The balanced temporal and spatial resolution of EEG/MEG has earned these techniques an indispensable position among existing tools for studying the spatiotemporal dynamics of large brain networks in humans.

4.2. Imaging Endogenous Event–Related and Spontaneous Brain Activity

ESI is also applicable to endogenous brain activity in normal and abnormal conditions. For motor imagery, a paradigm for the brain–computer interface (72, 73), ESI enhances the capability of decoding subjects' intent, relative to the direct use of sensor space signals (74, 75). The combination of ESI and fMRI data has also shed light on the nature of event-related (de)synchronization (76).

ESI has been widely used in epilepsy source localization, including interictal discharges (77–81). A study with more than 150 patients showed that source imaging using high-density EEG recordings has higher sensitivity and specificity than other imaging modalities, such as MRI and PET (78). When accurate forward models and high-density EEG caps are utilized, the location and dynamics of the epileptiform activities can be estimated to potentially inform clinical evaluation. Furthermore, ESI has been successfully used to localize seizures (82–84). Seizures are difficult to localize due to patients' head movement and consequently low signal-to-noise ratio. The oscillatory nature of seizure-related activity requires spatiotemporal ESI (83). The theta oscillation and its role in consciousness have also been characterized with ESI (85). **Figure 3** presents an example of seizure source imaging in partial epilepsy patients, validated against intracranial recordings or surgical outcome.

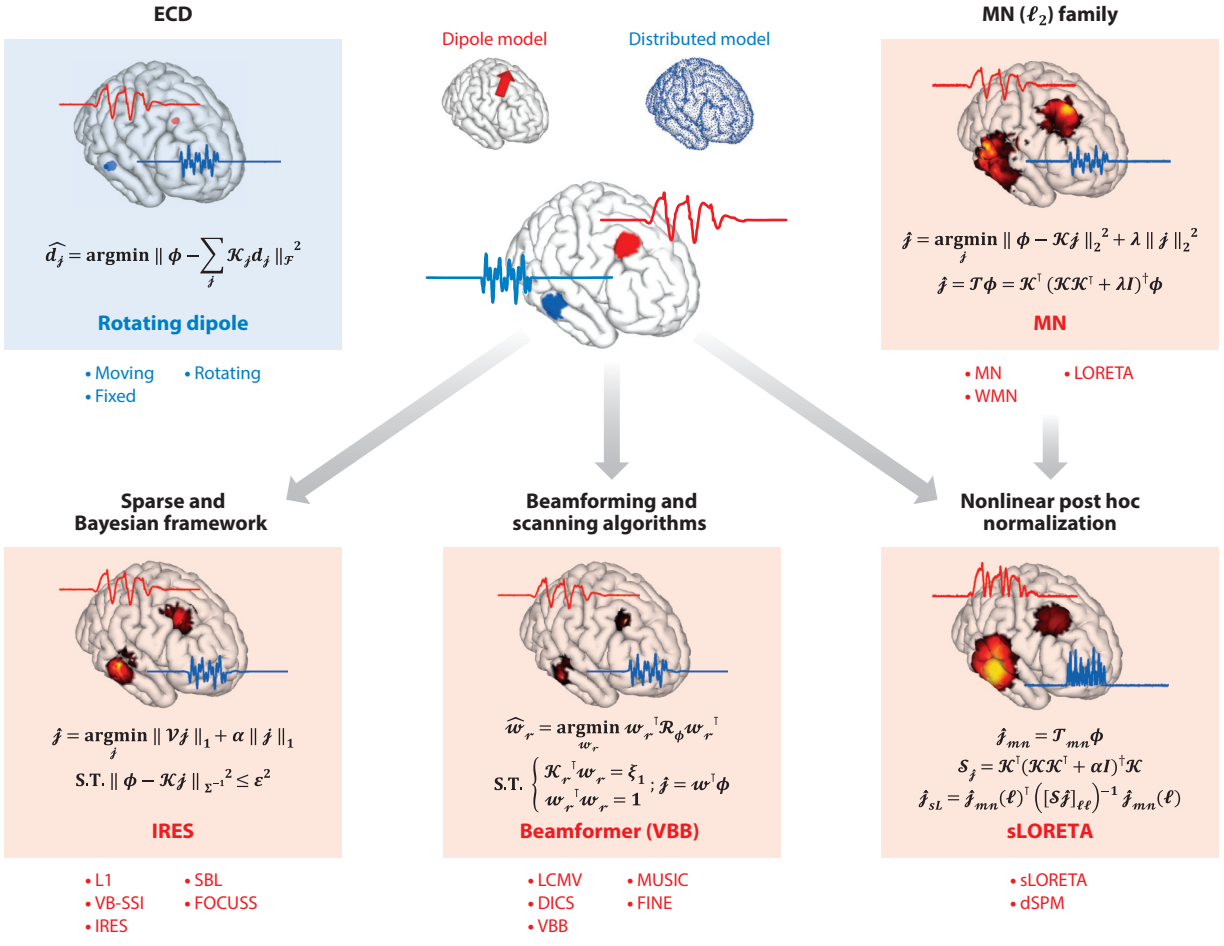

Figure 2

ESI at a glance. Different classes and families of source imaging algorithms are depicted. In the center, an underlying brain activity with two separate sources and the corresponding time course of the activity are simulated; the forward problem is solved, and the scalp potential distribution is calculated (simulated EEG). The solution of the dipole localization method for the given example is depicted on the top left. The rest of the figure shows the major families of inverse algorithms, and bulleted lists show some of the well-known algorithms in each family as examples (the lists are by no means exhaustive). For each case, the algorithm used to solve and produce the result is shown in bold red font under the result. The mathematical formulation for the algorithm is provided for each solution. The lead-field matrix (a transformation from the current dipole distribution to the scalp potential) is denoted by $\mathcal{K}$, the scalp potential as ϕ, the current density distribution as j, and the dipole moment as d_j (the lead-field entries corresponding to d_j are denoted by $\mathcal{K}_j$). The inverse imaging operator (for the MN family) is denoted by $\mathcal{T}$, and λ and α are regularization parameters. In the beamforming family, the data covariance is denoted by $\mathcal{R}_\phi$ and the spatial filter weights by w_r. For the IRES algorithm, $\mathcal{V}$ is the discrete gradient operator, Σ is the estimated noise covariance, and ε is the estimated noise power. Abbreviations: DICS, dynamic imaging of coherent sources; dSPM, dynamic statistical parametric mapping; ECD, equivalent current dipoles; EEG, electroencephalography; ESI, electrophysiological source imaging; FINE, first-principle vector; FOCUSS, focal undetermined system solution; IRES, iteratively reweighting edge sparsity; LCMV, linearly constrained minimum variance; LORETA, low-resolution electromagnetic tomography; MN, minimum norm; MUSIC, multiple classification algorithm; SBL, sparse Bayesian learning; sLORETA, standardized LORETA; VB-SSI, variation-based sparse source imaging; VBB, vector-based beamformer; WMN, weighted MN.

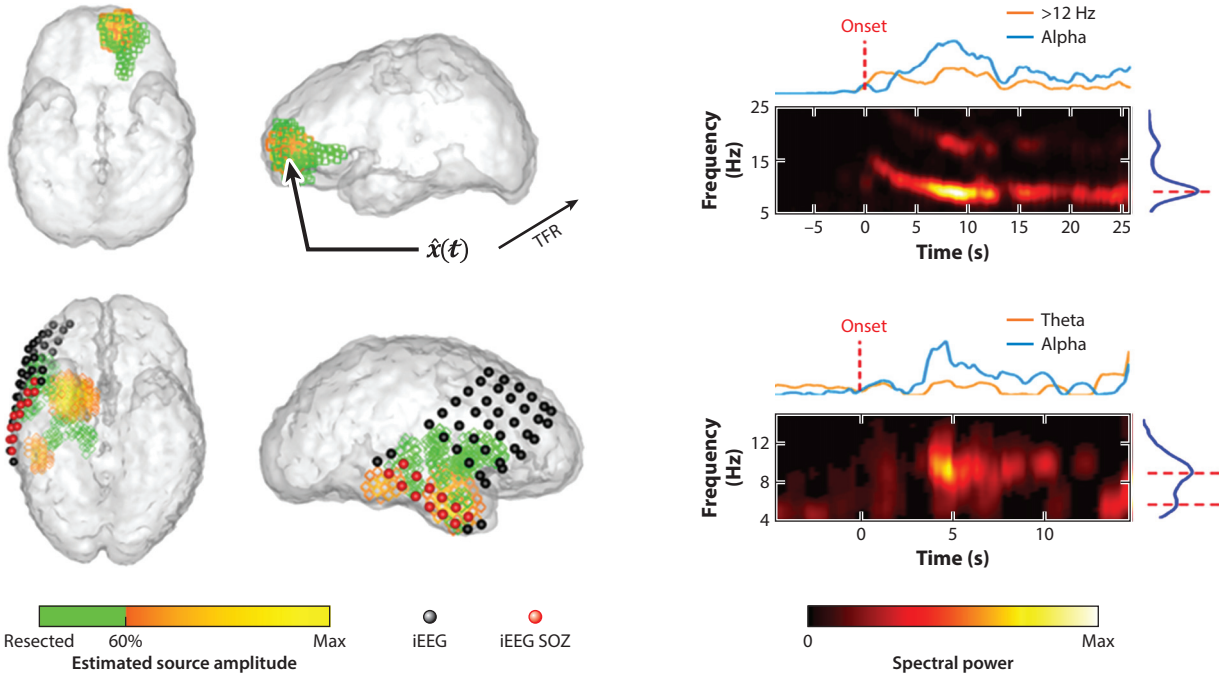

Figure 3

Electrophysiological source imaging of seizure. Seizure onset zones (SOZs) and the source time–frequency representations (TFRs) estimated from a typical seizure in (*top*) patient 1 with frontal lobe epilepsy and (*bottom*) patient 2 with temporal lobe epilepsy. The estimated SOZ (*yellow to orange color bar*) is colocalized with surgically resected zones (*green*) in patient 1 and with single-photon emission computed tomography (*green*) in patient 2. (*Right*) The TFRs show the time-frequency evolution at the maximal estimated SOZ point [the time course of activity derived at this location is labeled $\hat{x}(t)$]. Intracranial electrodes were implanted in patient 2 (*black spheres*), and SOZs were determined from intracranial seizure recordings (*red spheres*). Abbreviation: iEEG, intracranial EEG. Adapted with permission from Reference 83.

Another domain of applications for ESI includes imaging of ongoing and spontaneous brain activity. In the resting state, ESI has uncovered frequency-dependent functional networks and their dynamics (86–88). In disease states, ESI has revealed epileptic network characteristics (89, 90), even in the absence of epileptic activity.

5. IMAGING FUNCTIONAL CONNECTIVITY

Two concepts are essential to the brain's functional organization: functional segregation and integration (91). Whereas some brain regions or networks specialize in performing particular tasks, others integrate information (91), leading to complex cognition, behavior, or pathology. ESI can help understand and disentangle these processes (6).

5.1. Functional Versus Effective Connectivity

Functional connectivity concerns whether neural activity in a pair of regions (denoted A and B) is correlated or coherent (92, 93). Because correlation or coherence does not imply causation, functional connectivity does not report the directionality of the interaction between A and B. This sets functional connectivity apart from directional connectivity or effective connectivity (94),

which measures the causal relationship between A and B, as in Granger causality (95). Causality or directionality is often inferred from time series: If the past activity in A predicts the current or future activity in B, then A causes or drives B through connectivity from A to B (96).

5.2. Electrophysiological Connectome

ESI allows one to map functional/effective connectivity in source space—the concept of the electrophysiological connectome (eConnectome) (6, 97). Algorithms developed for estimating functional connectivity from electrophysiological source signals derived from EEG (or MEG) include the directed transfer function (DTF) algorithm (98) and the adaptive DTF (99–101), direct DTF (102), and partial directed coherence algorithms (103). The eConnectome approach (104, 105) has stirred interest in studying pathological networks such as epilepsy, in which determining the source of seizures is particularly important (106). MEG is also an effective tool for studying resting state functional connectivity and correlates well with fMRI studies with the added value of high temporal resolution (107). Such approaches have been used to determine epileptic networks with positive results, indicating the merits of integrating ESI with functional connectivity in mapping brain networks (108, 109). **Figure 4** schematically illustrates the eConnectome approach for mapping functional brain networks with ESI.

5.3. Dynamic Causal Modeling

The above-mentioned methods for directional connectivity are all data driven. Model-based connectivity techniques, such as dynamic causal modeling (DCM), have also attracted attention (110). Although DCM and Granger causality algorithms serve similar purposes, they are fundamentally different (111). Model-based methods depend on the choice of the model and its parameters; thus, many different parameters need to be tested to ensure unbiased results (112). This brings higher computational demand but may lead to valuable insights if the model and parameters are appropriately selected.

6. MULTIMODAL NEUROIMAGING

Where EEG/MEG fall short in neural imaging, fMRI excels, and vice versa. EEG/MEG can resolve neural events with high temporal resolution but limited spatial resolution (113); fMRI localizes brain activity with millimeter precision but cannot probe the rapidly changing neuronal dynamics (114). These complementary strengths and limitations have motivated researchers to integrate EEG/MEG and fMRI toward a multimodal imaging tool that is more powerful than each of them alone (115–117). The feasibility of concurrent EEG and fMRI acquisition makes EEG more preferable than MEG, especially for functional imaging in task-free or self-paced states that are hard to precisely replicate in separate experiments.

6.1. Synaptic Activity: The Common Origin of fMRI and EEG/MEG

The origin of fMRI is complex and incompletely understood (118). The most widely used fMRI signal, blood oxygenation level–dependent (BOLD) (119), is observable with rapid pulse sequences sensitized to the T_2^*-weighted contrast (120–122). What causes the BOLD effect is the varying concentration of deoxygenated hemoglobin relative to the total hemoglobin that is either deoxygenated or oxygenated (123). As neural activity elevates, local oxygen consumption and demand increases, triggering vasodilation of arterioles and capillaries to increase cerebral blood flow (124),

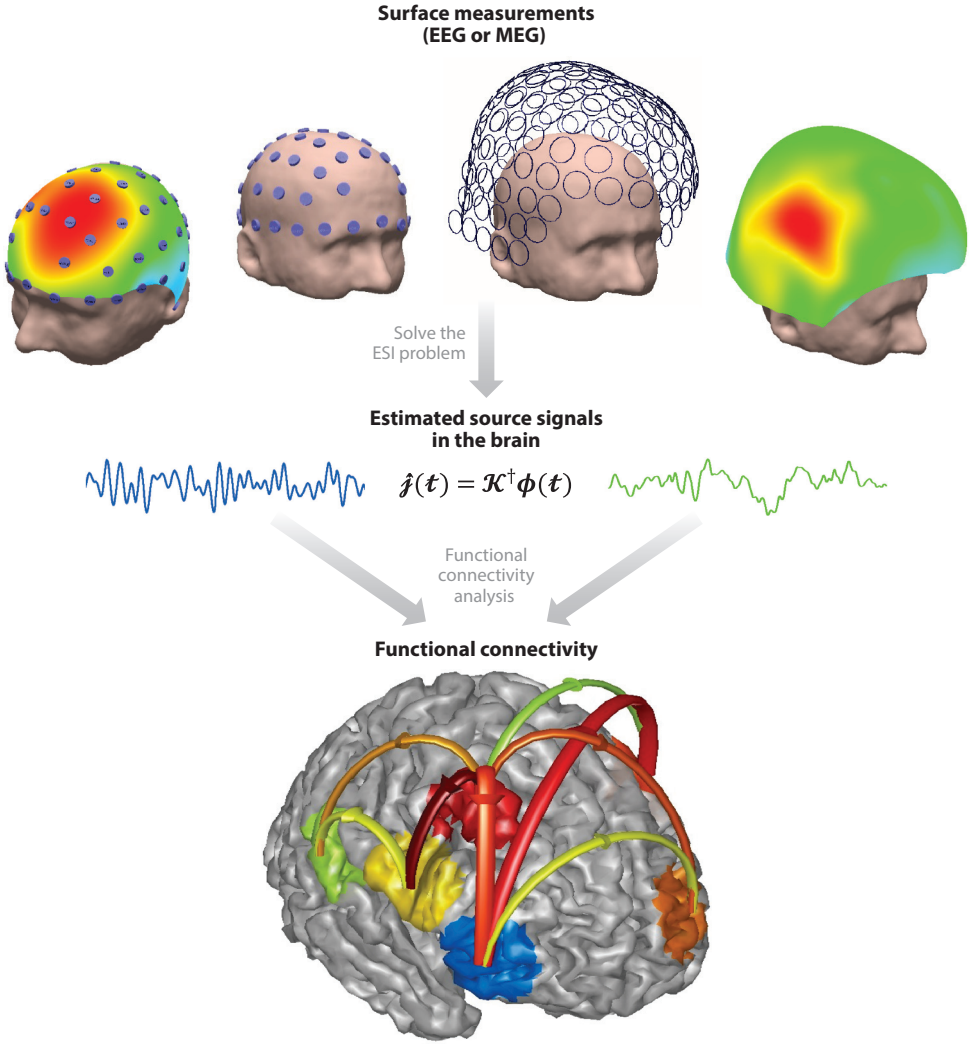

Figure 4

The concept of the electrophysiological connectome (eConnectome). Electrophysiological source imaging (ESI) can image not only brain activity but also the functional connectivity of the brain. The eConnectome approach estimates brain network dynamics from noninvasive surface techniques, such as electroencephalography (EEG) and magnetoencephalography (MEG). The location of the activity (nodes), the time course of the activity at such nodes, and the dynamic connectivity among these nodes (links) can be estimated from EEG/MEG to reveal the underlying brain networks. ESI is a key element in realizing this goal. The eConnectome is effective and accurate in imaging brain network dynamics in the source domain. Arrows (colored arrows on the cortical surface) represent the direction of information flow and directional functional connectivity or causality. The inversion operator is denoted by $\mathcal{K}^{\dagger}$, and the estimated current density distribution is denoted by $\hat{j}$.

which supplies oxygenated hemoglobin in excess of the metabolic rate of oxygen consumption (125). As a result, the concentration of deoxygenated hemoglobin decreases in capillary and venous vessels, reducing the paramagnetic susceptibility effect and thus increasing the T_2^*-weighted signal (123). Such a cascade of metabolic and vascular events, known as neurovascular coupling, involves complex signaling among neurons, astrocytes, and the local vasculature (124, 126, 127), and remains a topic of active research enabled by emerging tools (128).

The mechanism of neurovascular coupling is incompletely understood but essential to interpretation of fMRI (114, 118). Increasing evidence suggests that the primary source of the fMRI signal is synaptic activity, rather than spiking activity, in the gray matter (129, 130). In primates, synaptic activity consumes much more energy than action potentials (131); the gray matter is more densely vascularized than the white matter (132). As such, synaptic activity is a stronger driver of energy demand, and the gray matter vasculature further amplifies the metabolic fluctuation into an even greater vascular effect. Importantly, the synaptic contribution to the BOLD signal implies that fMRI and EEG/MEG may reflect highly distinct manifestations of the same physiological origin. Of synaptic activity in the gray matter, the metabolic and vascular effects give rise to the fMRI signal through neurovascular coupling with a severe loss of temporal specificity; the electromagnetic effect gives rise to EEG/MEG signals through head volume conduction with a severe loss of spatial specificity.

Studies that have directly compared fMRI and neural signals lend strong support to this idea (129, 130, 133–135). In neural signals, LFP reflects the synaptic input to a neuronal ensemble, and multiunit activity (MUA) reflects its spiking output. When recorded simultaneously during sensory stimulation, the BOLD response is more closely correlated with LFP than MUA (129, 130). After neuronal input and output are dissociated, the BOLD response is still correlated with LFP but not with MUA (133, 134). Although it is perhaps most notable in the gamma range, the LFP–BOLD correlation is not limited to any single frequency but rather spans a broad band (135). In the absence of any sensory input, spontaneous BOLD fluctuations are still correlated with underlying synaptic activity observed with LFP (136, 137), electrocorticography (138), and EEG (139, 140). Given these findings, it is reasonable to state that fMRI and EEG signals, to a large extent, share a common origin of cortical synaptic activity, but reflect its distribution and dynamics in highly different spatial and temporal scales with distinctive sensitivity, resolution, and specificity (141).

6.2. Joint Solutions to Two Inverse Problems

Most combined fMRI–EEG/MEG imaging methods are being developed in the context of two inverse problems. One is a spatially inverse problem, namely spatial localization of temporally resolved EEG/MEG signals (8, 142). The other is a temporally inverse problem, namely temporal decomposition of spatially resolved fMRI signals (143, 144). When fMRI is utilized to help solve the EEG/MEG inverse problem (i.e., fMRI-constrained EEG/MEG ESI), the solution benefits from the spatial precision and resolution of fMRI while inheriting the intrinsic temporal resolution of EEG/MEG (115, 117). When EEG is utilized to solve the fMRI inverse problem (i.e., EEG-informed fMRI), the solution benefits from the use of EEG to separate neural components or events in time or frequency while inheriting the intrinsic spatial resolution of fMRI (116, 140). What is preferable is a "symmetric" strategy to arrive at the estimation of a common set of unknown sources that simultaneously fit both fMRI and EEG measurements. Such a strategy is lacking despite initial progress (145), and awaits further quantitative understanding and modeling of the basis of and coupling between fMRI and EEG. **Figure 5** schematically illustrates the joint inverse problem of fMRI and EEG/MEG.

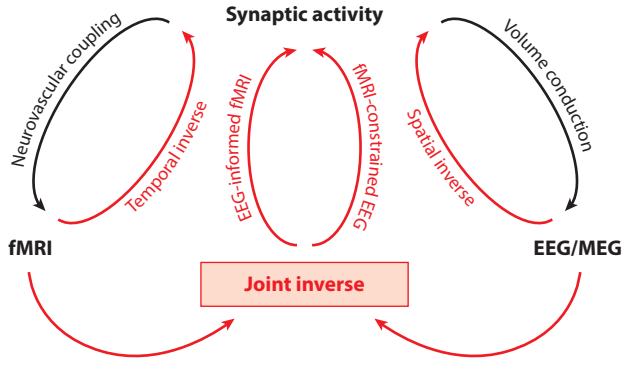

Figure 5

The common origin and the joint inverse solutions of functional magnetic resonance imaging (fMRI) and electroencephalography and magnetoencephalography (EEG/MEG). The spatially inverse problem refers to spatial localization and imaging of temporally resolved EEG/MEG signals. The temporally inverse problem refers to temporal decomposition of spatially resolved fMRI signals. Both fMRI and EEG (or MEG) have synaptic origins.

6.3. Using fMRI for the EEG/MEG Inverse Solution

fMRI-constrained EEG/MEG analysis has evolved from being mostly empirical to being progressively more principled. Perhaps the earliest and simplest method is to use fMRI activation foci to place multiple current dipoles, and then to fit the dipole moments to ERPs (146). The estimated time series of each dipole reports the response dynamics at the corresponding fMRI hot spot. Although overly simplified, this method is valuable in revealing the temporal sequence of task-evoked neural responses underlying perception or cognition (146, 147).

An alternative method is to improve the EEG/MEG-based estimation of cortical current density by using algorithms with fMRI-biased regularization (97, 148–150). Although they may be implemented in different theoretical frameworks, such as WMN (97), Wiener filter (149, 150), and Bayesian inference (43), all such algorithms share and utilize a common assumption that EEG/MEG sources are more likely to occur in locations that fMRI views as activated. The choice of the hyperparameter that controls the fMRI bias is often critical. This choice is mostly empirical for the lack of biophysical and quantitative interpretation of fMRI activation. In fMRI, a voxel being activated means that the voxel's signal is significantly different from noise and is predictable by the stimuli and tasks of interest. Note that this statistical meaning does not inform any physical characteristic about neuroelectric activity. A more rational choice requires further understanding and modeling of the relationships among EEG/MEG, fMRI, and stimuli.

It is feasible to model the relationship between fMRI and EEG/MEG given relatively simple stimuli that repeat as discrete events and/or in alternating blocks (115). For event-related or block-design paradigms, the size of the BOLD effect, given repeated stimuli on a long timescale, is approximately proportional to the integral of the power of stimulus-evoked synaptic activity in a short period following each stimulus (151). This relationship yields a quantitative model to relate fMRI to EEG/MEG, enabling a more principled way to use fMRI to constrain the EEG/MEG inverse solution for stimulus-evoked responses (150–152). However, this model fails to account for negative BOLD responses (153) or changes in spontaneous activity (154). The limitation is worth noting, given that spontaneous activity consumes most energy (155), drives BOLD fluctuations (143), and interacts with tasks or stimuli (156, 157).

6.4. Using EEG for the fMRI Inverse Solution

Compared with fMRI-constrained EEG/MEG inverse solutions, using EEG to inform fMRI mapping is more straightforward (140, 158). The central idea is to extract features from EEG and then relate them to the voxel-wise fMRI signal. With this idea, one may generate high-resolution activity maps presumably underlying the EEG features of interest (158), or address the EEG correlates to fMRI activity at specific voxels, regions, or networks (144, 159).

Features of EEG are often defined and extracted by frequencies or frequency bands (e.g., delta, theta, alpha, beta, and gamma). Different frequency components can be extracted by simply filtering EEG within narrow bands. Such band-pass filtered signals, often referred to as oscillations or rhythms, have been thought to bear important functional roles (160) and indicate brain states (161). Although the oscillation itself is too fast for fMRI to follow, its power or amplitude fluctuation falls in a similar time range as the fMRI signal (162). Correlation between the fMRI signal and the power fluctuation of an oscillation at a given frequency has been used to map the network that generates brain rhythms (140, 143). An excellent example is the alpha rhythm—a hallmark phenomenon in EEG. Studies have shown that the alpha-band power is correlated to the fMRI signal from visual and sensorimotor cortices (163), attention network (164, 165), and thalamic nuclei (166). The EEG–fMRI correlation in the thalamus demonstrates the synergistic merit of fMRI–EEG, because the thalamus is too far away to generate reliable EEG and localizing such deep sources with EEG alone is challenging. Other frequency bands have also been studied in a similar fashion; for example, studies have shown a negative coupling between frontal theta rhythm and the default-mode network (167).

Caution should be exercised when correlating the fMRI signal to a single-frequency component of EEG. This is because EEG, or its underlying neural activity, almost never manifests itself as a single-frequency rhythm; instead, it always contains a mixture of rhythms, and an arrhythmic component that follows a power-law ($1/f$) distribution across a broad band (168). Different frequency components are often related to one another such that the magnitude of one frequency is coupled to the magnitude or phase of another frequency (169). Therefore, it is important to consider all frequency components together as a collective account of the fMRI signal, while disentangling the differential contributions from broadband versus narrowband components (139, 170), as well as oscillations at different frequencies (171). In this regard, recent findings suggest that (broadband) arrhythmic and (narrowband) rhythmic processes account for global and modular patterns of functional connectivity observed with resting-state fMRI, respectively (170). The EEG correlates of resting-state networks exhibit distinct spectral signatures, characterizing the way by which neural oscillations support interregional interactions within networks (144, 159).

Features can also be extracted from EEG as characteristic spatial patterns or microstates that reoccur over time (8, 172). The EEG microstates correlate with the fMRI signal in the resting state (173–175). Moreover, for event-like tasks or stimuli, EEG features may also be extracted from temporal variations in single-trial potentials, and their correlations with fMRI reveal rich temporal dynamics of information processing in task-evoked neural networks (176, 177).

6.5. Challenges and Opportunities

A critical challenge for integrating fMRI and EEG is the strong electromagnetic interference that causes artifacts in simultaneously acquired fMRI and EEG signals (178). The artifacts are of greater concern for EEG than for fMRI, and tend to deteriorate in higher fields (179). Existing ways of removing such recording artifacts are mostly in postprocessing algorithms (180). Hardware

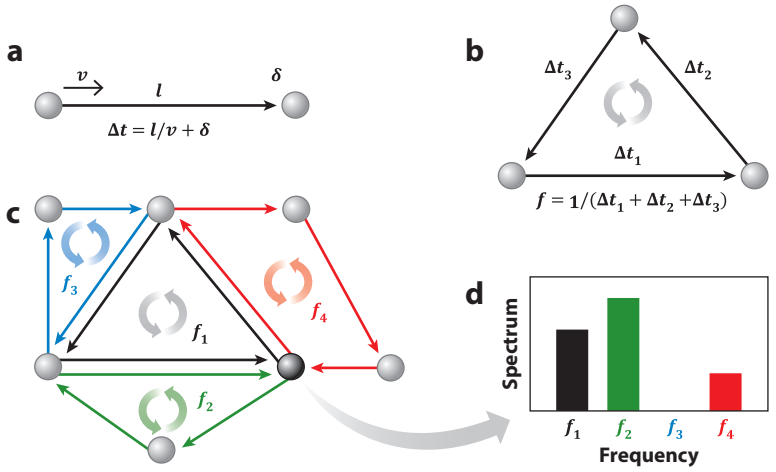

Figure 6

The structure–function relationship in spectral signatures of brain activity and connectivity observable with functional magnetic resonance imaging combined with electroencephalography and magnetoencephalography (fMRI–EEG/MEG). (*a*) The time delay (Δt) between two interconnected regions depends on the axonal length (l), conduction velocity (v), and synaptic delay (δ). (*b*) The cumulative delay of a circular path entails the sum of delays via every path, and contributes to network dynamics at one specific frequency. (*c*) A region can be involved in multiple circuits with distinct frequencies (f). (*d*) The spectrum at this region indicates its relative involvements in all circuits for a given period.

solutions that reduce or eliminate the artifacts are needed for broader and more routine applications of fMRI–EEG. Initial progress is encouraging and merits further development (181).

Combining fMRI and EEG serves to bridge brain signals across spatial and temporal scales. Questions remain as to how functional information reported with fMRI–EEG relates to the brain's structural characteristics, the roles of different neuronal circuits, and the excitation–inhibition balance. Such questions are approachable from multiple perspectives.

For example, the relationships between fMRI and EEG in distinct frequencies likely reflect the spectral signatures of regional activity and interregional interaction (144, 182, 183). Such spectral signatures may be closely related to the topological properties of structural connectivity. Neuronal communication takes time, depending on the distance and the velocity of signaling between neurons (**Figure 6*a***). The frequency of neuronal oscillation is inversely related to the cumulative time delay for information to travel out of a region and back to itself through an indirect polysynaptic pathway (**Figure 6*b***). Because a region is involved in many such recurrent pathways with various time delays (**Figure 6*c***), the spectrum of regional activity should indicate the histogram of the time delays of all structural circuits in which this region is actively involved for a given period of time (**Figure 6*d***). It is plausible to predict that when a region (or a pair of regions) is engaged in relatively local-scale processing, it tends to involve shorter pathways and less synapses, giving rise to shorter time periods; thus, higher-frequency components will be more evident. Such interpretation and prediction remain to be tested, but represent a plausible scenario about the fundamental relationships between circuit structures and dynamics.

Spectral information obtained from EEG/MEG or EEG–fMRI may be interpreted in relation to feedforward and feedback pathways. Recent studies suggest that the frequency of neural oscillations marks the directionality of network interactions: Low-frequency oscillations (e.g., alpha) reflect feedback processes, and high-frequency oscillations (e.g., gamma) reflect feedforward

OPEN-SOURCE ESI SOFTWARE

ESI algorithms are widely available to the public via free and open-source software. Some of the toolboxes that are capable of performing source imaging as well as connectivity analysis include eConnectome (104), FieldTrip (199), MNE (200), and Nutmeg (201); others, such as BrainStorm (202), focus mainly on source imaging. Some toolboxes are more specialized for time-series and component analysis, such as EEGLAB (203), and some specialize in scalp topographical analysis and clustering, such as CARTOOL (204). The widely used statistical parameter mapping (SPM) toolbox (205, 206) was developed initially for fMRI and DCM analysis and now includes EEG/MEG analysis. Additional toolboxes, such as the partial directed coherence (207) and source information flow (208) toolboxes, specialize in connectivity analysis and not as much on source imaging.

Subject-specific head models, usually derived from the subject's MRI, are necessary to solve the forward problem and are ultimately used in ESI; such toolboxes include FreeSurfer (209), BrainSuite (210), and BrainVISA Anatomist (211). OpenMEEG (212) can be used to make subject-specific BEM models.

Many more freely available open-source toolboxes are online, in addition to commercial software. We present only a few examples of the better-known toolboxes to guide the reader. All of the toolboxes introduced above have extensive online tutorials and user guides and are relatively easy to set up and work with.

processes (184–186). Such findings are consistent with the observable laminar profile of fMRI (187), LFP-based phase relationships (184), and effects of neuromodulation (188). Although the findings need further replication and validation, conceivable implications include using the frequency information to infer directional networks and to investigate the dynamics and roles of feedforward versus feedback pathways against theories in computational neuroscience, such as predictive coding (189, 190) and free-energy principles (191).

7. CONCLUSIONS AND FUTURE TRENDS

EEG and MEG are noninvasive techniques that record brain electromagnetic activity with high temporal resolution. Once ESI is applied to high-density EEG/MEG recordings, brain electrical activity can be imaged with sublobar resolution on the order of ~5 mm, on the level of cortical gyri and sulci (192). ESI also disentangles sensor-level signals to reveal electrophysiological dynamics in regional activity or interregional connectivity, yielding new insights into brain functions in health (193) and disease (194–196).

Given its current advances and continuing development, ESI will increasingly be used for clinical applications. The inexpensive EEG setups available in most clinical settings, the availability of computers, and the accessible open-source ESI analysis tools (see the sidebar titled Open-Source ESI Software) will enable broad applications of EEG source imaging. Furthermore, the capability of imaging dynamic brain activity from the whole brain makes ESI a desirable means for studying large-scale brain networks in humans.

While ESI can provide highly valuable information about brain networks and dynamics, it also has the advantage of being integrated with other modalities, such as fMRI, to combine the high temporal resolution of EEG with the high spatial resolution of fMRI (see Section 6). Efforts to increase the spatiotemporal resolution in imaging brain function are ongoing (197). It is envisioned that developments in designing better ESI algorithms, and combining EEG/MEG with other neural imaging or modulation techniques, such as transcranial focus ultrasound (198), will be at the frontier of advances in functional neuroimaging.

DISCLOSURE STATEMENT

The authors are not aware of any affiliations, memberships, funding, or financial holdings that might be perceived as affecting the objectivity of this review.

ACKNOWLEDGMENTS

The writing of this review was supported in part by National Institutes of Health grants EB021027, NS096761, MH114233, AT009263, EY023101, MH104402, EB008389, and HL117664 and by National Science Foundation grants CBET-1450956 and DGE-1069104.

LITERATURE CITED

1. Herculano-Houzel S. 2009. The human brain in numbers: a linearly scaled-up primate brain. *Front. Hum. Neurosci.* 3:1–11
2. Pakkenberg B, Pelvig D, Marner L, Bundgaard MJ, Gundersen HJG, et al. 2003. Aging and the human neocortex. *Exp. Gerontol.* 38:95–99
3. Nunez PL, Srinivasan R. 2006. *Electric Fields of the Brain: The Neurophysics of EEG*. New York: Oxford Univ. Press
4. He B, Ding L. 2013. Electrophysiological mapping and neuroimaging. In *Neural Engineering*, ed. B He, pp. 499–543. Berlin: Springer
5. Plonsey R. 1969. *Bioelectric Phenomena*. New York: McGraw-Hill
6. He B, Yang L, Wilke C, Yuan H. 2011. Electrophysiological imaging of brain activity and connectivity—challenges and opportunities. *Biomed. Eng. IEEE Trans.* 58:1918–31
7. Malmivuo J, Plonsey R. 1995. *Bioelectromagnetism: Principles and Applications of Bioelectric and Biomagnetic Fields*. New York: Oxford Univ. Press
8. Michel CM, He B. 2011. EEG mapping and source imaging. In *Niedermeyer's Electroencephalography: Basic Principles, Clinical Applications, and Related Fields*, ed. DL Schomer, FH Lopes da Silva, pp. 1179–202. Philadelphia: Lippincott Williams & Wilkins. 6th ed.
9. Lopes da Silva FH, Van Rotterdam AB. 2011. Biophysical aspects of EEG and magnetoencephalography generation. In *Niedermeyer's Electroencephalography: Basic Principles, Clinical Applications, and Related Fields*, ed. DL Schomer, FH Lopes da Silva, pp. 91–110. Philadelphia: Lippincott Williams & Wilkins. 6th ed.
10. Riera JJ, Ogawa T, Goto T, Sumiyoshi A, Nonaka H, et al. 2012. Pitfalls in the dipolar model for the neocortical EEG sources. *J. Neurophysiol.* 108:956–75
11. Jerbi K, Mosher JC, Baillet S, Leahy RM. 2002. On MEG forward modelling using multipolar expansions. *Phys. Med. Biol.* 47:523–55
12. Ding L, Zhang N, Chen W, He B. 2009. Three-dimensional imaging of complex neural activation in humans from EEG. *IEEE Trans. Biomed. Eng.* 56:1980–88
13. He B, Musha T, Okamoto Y, Homma S, Nakajima Y, Sato T. 1987. Electric dipole tracing in the brain by means of the boundary element method and its accuracy. *IEEE Trans. Biomed. Eng.* 6:406–14
14. Hamalainen MS, Sarvas J. 1989. Realistic conductivity geometry model of the human head for interpretation of neuromagnetic data. *Biomed. Eng. IEEE Trans.* 36:165–71
15. Yan Y, Nunez PL, Hart RT. 1991. Finite-element model of the human head: scalp potentials due to dipole sources. *Med. Biol. Eng. Comput.* 29:475–81
16. von Helmholtz H. 1853. Über einige Gesetze der Vertheilung elektrischer Ströme in körperlichen Leitern mit Anwendung auf die thierisch-elektrischen Versuche. *Ann. Phys.* 165:211–33
17. Hansen PC. 1992. Analysis of discrete ill-posed problems by means of the L-curve. *SIAM Rev.* 34:561–80
18. Lantz G, de Peralta RG, Spinelli L, Seeck M, Michel CM. 2003. Epileptic source localization with high density EEG: How many electrodes are needed? *Clin. Neurophysiol.* 114:63–69
19. Sohrabpour A, Lu Y, Kankirawatana P, Blount J, Kim H, He B. 2015. Effect of EEG electrode number on epileptic source localization in pediatric patients. *Clin. Neurophysiol.* 126:472–80

20. Seeck M, Koessler L, Bast T, Leijten F, Michel C, et al. 2017. The standardized EEG electrode array of the IFCN. *Clin. Neurophysiol.* 128:2070–77
21. Scherg M, Von Cramon D. 1985. Two bilateral sources of the late AEP as identified by a spatio-temporal dipole model. *Electroencephalogr. Clin. Neurophysiol.* 62:32–44
22. Ebersole JS. 1991. EEG dipole modeling in complex partial epilepsy. *Brain Topogr.* 4:113–23
23. Dale AM, Sereno MI. 1993. Improved localizadon of cortical activity by combining EEG and MEG with MRI cortical surface reconstruction: a linear approach. *J. Cogn. Neurosci.* 5:162–76
24. Hämäläinen MS, Ilmoniemi RJ. 1994. Interpreting magnetic fields of the brain: minimum norm estimates. *Med. Biol. Eng. Comput.* 32:35–42
25. Wang J-Z, Williamson SJ, Kaufman L. 1992. Magnetic source images determined by a lead-field analysis: the unique minimum-norm least-squares estimation. *IEEE Trans. Biomed. Eng.* 39:665–75
26. Lawson CL, Hanson RJ. 1995. *Solving Least Squares Problems*. Philadelphia: SIAM
27. Greenblatt RE. 1993. Probabilistic reconstruction of multiple sources in the bioelectromagnetic inverse problem. *Inverse Probl.* 9:271
28. Fuchs M, Wischmann HA, Wagner M. 1994. Generalized minimum norm least squares reconstruction algorithms. *ISBET Newsl.* 5:8–11
29. Pascual-Marqui RD, Michel CM, Lehmann D. 1994. Low resolution electromagnetic tomography: a new method for localizing electrical activity in the brain. *Int. J. Psychophysiol.* 18:49–65
30. Pascual-Marqui RD. 2002. Standardized low-resolution brain electromagnetic tomography (sLORETA): technical details. *Methods Find. Exp. Clin. Pharmacol.* 24(Suppl. D):5–12
31. Molins A, Stufflebeam SM, Brown EN, Hämäläinen MS. 2008. Quantification of the benefit from integrating MEG and EEG data in minimum ℓ 2-norm estimation. *NeuroImage* 42:1069–77
32. Van Veen BD, Buckley KM. 1988. Beamforming: a versatile approach to spatial filtering. *IEEE ASSP Mag.* 5:4–24
33. Van Veen BD, Van Drongelen W, Yuchtman M, Suzuki A. 1997. Localization of brain electrical activity via linearly constrained minimum variance spatial filtering. *IEEE Trans. Biomed. Eng.* 44:867–80
34. Baillet S, Mosher JC, Leahy RM. 2001. Electromagnetic brain mapping. *IEEE Signal Process. Mag.* 18:14–30
35. Sekihara K, Nagarajan SS, Poeppel D, Marantz A, Miyashita Y. 2001. Reconstructing spatio-temporal activities of neural sources using an MEG vector beamformer technique. *IEEE Trans. Biomed. Eng.* 48:760–71
36. Gross J, Kujala J, Hämäläinen M, Timmermann L, Schnitzler A, Salmelin R. 2001. Dynamic imaging of coherent sources: studying neural interactions in the human brain. *PNAS* 98:694–99
37. Robinson SE, Vrba J. 1998. Functional neuroimaging by synthetic aperture magnetometry (SAM). In *Recent Advances in Biomagnetism*, ed. T Yoshimoto, M Kotani, S Kuriki, H Karibe, H Nahasato, pp. 302–5. Sandai, Jpn.: Tokyo Univ. Press
38. Mosher JC, Lewis PS, Leahy RM. 1992. Multiple dipole modeling and localization from spatio-temporal MEG data. *IEEE Trans. Biomed. Eng.* 39:541–57
39. Schmidt R. 1986. Multiple emitter location and signal parameter estimation. *IEEE Trans. Antennas Propag.* 34:276–80
40. Mosher JC, Leahy RM. 1999. Source localization using recursively applied and projected (RAP) MUSIC. *IEEE Trans. Signal Process.* 47:332–40
41. Xu X-L, Xu B, He B. 2004. An alternative subspace approach to EEG dipole source localization. *Phys. Med. Biol.* 49:327
42. Wipf D, Nagarajan S. 2009. A unified Bayesian framework for MEG/EEG source imaging. *NeuroImage* 44:947–66
43. Bolstad A, Van Veen B, Nowak R. 2009. Space-time event sparse penalization for magneto-/electroencephalography. *NeuroImage* 46:1066–81
44. Friston K, Harrison L, Daunizeau J, Kiebel S, Phillips C, et al. 2008. Multiple sparse priors for the M/EEG inverse problem. *NeuroImage* 39:1104–20
45. Trujillo-Barreto NJ, Aubert-Vázquez E, Valdés-Sosa PA. 2004. Bayesian model averaging in EEG/MEG imaging. *NeuroImage* 21:1300–19

46. Trujillo-Barreto NJ, Aubert-Vázquez E, Penny WD. 2008. Bayesian M/EEG source reconstruction with spatio-temporal priors. *NeuroImage* 39:318–35
47. Henson RN, Flandin G, Friston KJ, Mattout J. 2010. A parametric empirical Bayesian framework for fMRI-constrained MEG/EEG source reconstruction. *Hum. Brain Mapp.* 31:1512–31
48. Wipf DP, Owen JP, Attias HT, Sekihara K, Nagarajan SS. 2010. Robust Bayesian estimation of the location, orientation, and time course of multiple correlated neural sources using MEG. *NeuroImage* 49:641–55
49. Grova C, Daunizeau J, Lina J-M, Bénar CG, Benali H, Gotman J. 2006. Evaluation of EEG localization methods using realistic simulations of interictal spikes. *NeuroImage* 29:734–53
50. Lamus C, Hämäläinen MS, Temereanca S, Brown EN, Purdon PL. 2012. A spatiotemporal dynamic distributed solution to the MEG inverse problem. *NeuroImage* 63:894–909
51. Gorodnitsky IF, George JS, Rao BD. 1995. Neuromagnetic source imaging with FOCUSS: a recursive weighted minimum norm algorithm. *Electroencephalogr. Clin. Neurophysiol.* 95:231–51
52. Ding L, He B. 2008. Sparse source imaging in electroencephalography with accurate field modeling. *Hum. Brain Mapp.* 29:1053–67
53. Haufe S, Nikulin VV, Ziehe A, Müller K-R, Nolte G. 2008. Combining sparsity and rotational invariance in EEG/MEG source reconstruction. *NeuroImage* 42:726–38
54. Gramfort A, Strohmeier D, Haueisen J, Hämäläinen MS, Kowalski M. 2013. Time-frequency mixed-norm estimates: sparse M/EEG imaging with non-stationary source activations. *NeuroImage* 70:410–22
55. Sohrabpour A, Lu Y, Worrell G, He B. 2016. Imaging brain source extent from EEG/MEG by means of an iteratively reweighted edge sparsity minimization (IRES) strategy. *NeuroImage* 142:27–42
56. Ding L. 2009. Reconstructing cortical current density by exploring sparseness in the transform domain. *Phys. Med. Biol.* 54:2683
57. Donoho DL. 2006. Compressed sensing. *IEEE Trans. Inf. Theory* 52:1289–306
58. Matsuura K, Okabe Y. 1995. Selective minimum-norm solution of the biomagnetic inverse problem. *IEEE Trans. Biomed. Eng.* 42:608–15
59. Uutela K, Hämäläinen M, Somersalo E. 1999. Visualization of magnetoencephalographic data using minimum current estimates. *NeuroImage* 10:173–80
60. Wagner M, Wischmann H-A, Fuchs M, Köhler T, Drenckhahn R. 2000. Current density reconstructions using the L1 norm. In *Biomag 96: Proceedings of the 10th International Conference on Biomagnetism*, ed. CJ Aine, G Stroink, CC Wood, Y Okada, SJ Swithenby, pp. 393–96. Berlin: Springer
61. Fuchs M, Wagner M, Köhler T, Wischmann H-A. 1999. Linear and nonlinear current density reconstructions. *J. Clin. Neurophysiol.* 16:267–95
62. Liao K, Zhu M, Ding L, Valette S, Zhang W, Dickens D. 2012. Sparse representation of cortical current density maps using wavelets. *Phys. Med. Biol.* 57:6881–901
63. Zhu M, Zhang W, Dickens DL, Ding L. 2014. Reconstructing spatially extended brain sources via enforcing multiple transform sparseness. *NeuroImage* 86:280–93
64. Chang W-T, Nummenmaa A, Hsieh J-C, Lin F-H. 2010. Spatially sparse source cluster modeling by compressive neuromagnetic tomography. *NeuroImage* 53:146–60
65. Bar M, Kassam KS, Ghuman AS, Boshyan J, Schmid AM, et al. 2006. Top-down facilitation of visual recognition. *PNAS* 103:449–54
66. Khan S, Gramfort A, Shetty NR, Kitzbichler MG, Ganesan S, et al. 2013. Local and long-range functional connectivity is reduced in concert in autism spectrum disorders. *PNAS* 110:3107–12
67. Sergent C, Baillet S, Dehaene S. 2005. Timing of the brain events underlying access to consciousness during the attentional blink. *Nat. Neurosci.* 8:1391–400
68. Jamison KW, Roy AV, He S, Engel SA, He B. 2015. SSVEP signatures of binocular rivalry during simultaneous EEG and fMRI. *J. Neurosci. Methods* 243:53–62
69. Roy AV, Jamison KW, He S, Engel SA, He B. 2017. Deactivation in the posterior mid-cingulate cortex reflects perceptual transitions during binocular rivalry: evidence from simultaneous EEG-fMRI. *NeuroImage* 152:1–11
70. Zhang P, Jamison K, Engel S, He B, He S. 2011. Binocular rivalry requires visual attention. *Neuron* 71:362–69

71. Ahissar E, Nagarajan S, Ahissar M, Protopapas A, Mahncke H, Merzenich MM. 2001. Speech comprehension is correlated with temporal response patterns recorded from auditory cortex. *PNAS* 98:13367–72
72. He B, Gao S, Yuan H, Wolpaw JR. 2013. Brain–computer interfaces. In *Neural Engineering*, ed. B He, pp. 87–151. Berlin: Springer
73. He B, Baxter B, Edelman BJ, Cline CC, Wenjing WY. 2015. Noninvasive brain–computer interfaces based on sensorimotor rhythms. *Proc. IEEE.* 103:907–25
74. Qin L, Ding L, He B. 2004. Motor imagery classification by means of source analysis for brain-computer interface applications. *J. Neural Eng.* 1:65–72
75. Edelman BJ, Baxter B, He B. 2016. EEG source imaging enhances the decoding of complex right-hand motor imagery tasks. *IEEE Trans. Biomed. Eng.* 63:4–14
76. Yuan H, Liu T, Szarkowski R, Rios C, Ashe J, He B. 2010. Negative covariation between task-related responses in α/β-band activity and BOLD in human sensorimotor cortex: an EEG and fMRI study of motor imagery and movements. *NeuroImage* 49:2596–606
77. Lai Y, Zhang X, van Drongelen W, Korhman M, Hecox K, et al. 2011. Noninvasive cortical imaging of epileptiform activities from interictal spikes in pediatric patients. *NeuroImage* 54:244–52
78. Brodbeck V, Spinelli L, Lascano AM, Wissmeier M, Vargas M-I, et al. 2011. Electroencephalographic source imaging: a prospective study of 152 operated epileptic patients. *Brain* 134:2887–97
79. Shiraishi H, Ahlfors SP, Stufflebeam SM, Takano K, Okajima M, et al. 2005. Application of magnetoencephalography in epilepsy patients with widespread spike or slow-wave activity. *Epilepsia* 46:1264–72
80. Ossadtchi A, Baillet S, Mosher JC, Thyerlei D, Sutherling W, Leahy RM. 2004. Automated interictal spike detection and source localization in magnetoencephalography using independent components analysis and spatio-temporal clustering. *Clin. Neurophysiol.* 115:508–22
81. Kirsch HE, Robinson SE, Mantle M, Nagarajan S. 2006. Automated localization of magnetoencephalographic interictal spikes by adaptive spatial filtering. *Clin. Neurophysiol.* 117:2264–71
82. Ding L, Worrell GA, Lagerlund TD, He B. 2007. Ictal source analysis: localization and imaging of causal interactions in humans. *NeuroImage* 34:575–86
83. Yang L, Wilke C, Brinkmann B, Worrell GA, He B. 2011. Dynamic imaging of ictal oscillations using non-invasive high-resolution EEG. *NeuroImage* 56:1908–17
84. Lu Y, Yang L, Worrell GA, Brinkmann B, Nelson C, He B. 2012. Dynamic imaging of seizure activity in pediatric epilepsy patients. *Clin. Neurophysiol.* 123:2122–29
85. Yang L, Worrell GA, Nelson C, Brinkmann B, He B. 2012. Spectral and spatial shifts of post-ictal slow waves in temporal lobe seizures. *Brain* 135:3134–43
86. Hillebrand A, Barnes GR, Bosboom JL, Berendse HW, Stam CJ. 2012. Frequency-dependent functional connectivity within resting-state networks: an atlas-based MEG beamformer solution. *NeuroImage* 59:3909–21
87. Brookes MJ, Woolrich M, Luckhoo H, Price D, Hale JR, et al. 2011. Investigating the electrophysiological basis of resting state networks using magnetoencephalography. *PNAS* 108:16783–88
88. de Pasquale F, Penna SD, Snyder AZ, Lewis C, Mantini D, et al. 2010. Temporal dynamics of spontaneous MEG activity in brain networks. *PNAS* 107:6040–45
89. Coito A, Michel CM, van Mierlo P, Vulliémoz S, Plomp G. 2016. Directed functional brain connectivity based on EEG source imaging: methodology and application to temporal lobe epilepsy. *IEEE Trans. Biomed. Eng.* 63:2619–28
90. Haneef Z, Lenartowicz A, Yeh HJ, Levin HS, Engel J, Stern JM. 2014. Functional connectivity of hippocampal networks in temporal lobe epilepsy. *Epilepsia* 55:137–45
91. Friston KJ. 2011. Functional and effective connectivity: a review. *Brain Connect.* 1:13–36
92. Friston KJ. 1994. Functional and effective connectivity in neuroimaging: a synthesis. *Hum. Brain Mapp.* 2:56–78
93. Horwitz B. 2003. The elusive concept of brain connectivity. *NeuroImage* 19:466–70
94. Friston KJ. 2009. Modalities, modes, and models in functional neuroimaging. *Science* 326:399–403
95. Granger CWJ. 1969. Investigating causal relations by econometric models and cross-spectral methods. *Econometrica* 37:424–38
96. Geweke J. 1982. Measurement of linear dependence and feedback between multiple time series. *J. Am. Stat. Assoc.* 77:304–13

97. Babiloni F, Cincotti F, Babiloni C, Carducci F, Mattia D, et al. 2005. Estimation of the cortical functional connectivity with the multimodal integration of high-resolution EEG and fMRI data by directed transfer function. *NeuroImage* 24:118–31
98. Kaminski MJ, Blinowska KJ. 1991. A new method of the description of the information flow in the brain structures. *Biol. Cybern.* 65:203–10
99. Ding M, Bressler SL, Yang W, Liang H. 2000. Short-window spectral analysis of cortical event-related potentials by adaptive multivariate autoregressive modeling: data preprocessing, model validation, and variability assessment. *Biol. Cybern.* 83:35–45
100. Wilke C, Ding L, He B. 2008. Estimation of time-varying connectivity patterns through the use of an adaptive directed transfer function. *Biomed. Eng. IEEE Trans.* 55:2557–64
101. Astolfi L, Cincotti F, Mattia D, Fallani FDV, Tocci A, et al. 2008. Tracking the time-varying cortical connectivity patterns by adaptive multivariate estimators. *IEEE Trans. Biomed. Eng.* 55:902–13
102. Korzeniewska A, Mańczak M, Kamiński M, Blinowska KJ, Kasicki S. 2003. Determination of information flow direction among brain structures by a modified directed transfer function (dDTF) method. *J. Neurosci. Methods* 125:195–207
103. Baccalá LA, Sameshima K. 2001. Partial directed coherence: a new concept in neural structure determination. *Biol. Cybern.* 84:463–74
104. He B, Dai Y, Astolfi L, Babiloni F, Yuan H, Yang L. 2011. eConnectome: a MATLAB toolbox for mapping and imaging of brain functional connectivity. *J. Neurosci. Methods* 195:261–69
105. Sohrabpour A, Ye S, Worrell GA, Zhang W, He B. 2016. Noninvasive electromagnetic source imaging and granger causality analysis: an electrophysiological connectome (eConnectome) approach. *IEEE Trans. Biomed. Eng.* 63:2474–87
106. Lu Y, Yang L, Worrell GA, He B. 2012. Seizure source imaging by means of FINE spatio-temporal dipole localization and directed transfer function in partial epilepsy patients. *Clin. Neurophysiol.* 123:1275–83
107. Brookes MJ, Hale JR, Zumer JM, Stevenson CM, Francis ST, et al. 2011. Measuring functional connectivity using MEG: methodology and comparison with fcMRI. *NeuroImage* 56:1082–104
108. Elisevich K, Shukla N, Moran JE, Smith B, Schultz L, et al. 2011. An assessment of MEG coherence imaging in the study of temporal lobe epilepsy. *Epilepsia* 52:1110–19
109. Englot DJ, Hinkley LB, Kort NS, Imber BS, Mizuiri D, et al. 2015. Global and regional functional connectivity maps of neural oscillations in focal epilepsy. *Brain* 138:2249–62
110. Friston KJ, Harrison L, Penny W. 2003. Dynamic causal modelling. *NeuroImage* 19:1273–302
111. Friston K, Moran R, Seth AK. 2013. Analysing connectivity with Granger causality and dynamic causal modelling. *Curr. Opin. Neurobiol.* 23:172–78
112. Daunizeau J, David O, Stephan KE. 2011. Dynamic causal modelling: a critical review of the biophysical and statistical foundations. *NeuroImage* 58:312–22
113. Baillet S. 2017. Magnetoencephalography for brain electrophysiology and imaging. *Nat. Neurosci.* 20:327–39
114. Logothetis NK. 2008. What we can do and what we cannot do with fMRI. *Nature* 453:869–78
115. He B, Liu Z. 2008. Multimodal functional neuroimaging: integrating functional MRI and EEG/MEG. *IEEE Rev. Biomed. Eng.* 1:23–40
116. Ritter P, Villringer A. 2006. Simultaneous EEG-fMRI. *Neurosci. Biobehav. Rev.* 30:823–38
117. Liu Z, Ding L, He B. 2006. Integration of EEG/MEG with MRI and fMRI. *IEEE Eng. Med. Biol. Mag.* 25:46–53
118. Kim S-G, Ogawa S. 2012. Biophysical and physiological origins of blood oxygenation level–dependent fMRI signals. *J. Cereb. Blood Flow Metab.* 32:1188–206
119. Ogawa S, Lee TM, Kay AR, Tank DW. 1990. Brain magnetic resonance imaging with contrast dependent on blood oxygenation. *PNAS* 87:9868–72
120. Bandettini PA, Wong EC, Hinks RS, Tikofsky RS, Hyde JS. 1992. Time course EPI of human brain function during task activation. *Magn. Reson. Med.* 25:390–97
121. Kwong KK, Belliveau JW, Chesler DA, Goldberg IE, Weisskoff RM, et al. 1992. Dynamic magnetic resonance imaging of human brain activity during primary sensory stimulation. *PNAS* 89:5675–79
122. Ogawa S, Tank DW, Menon R, Ellermann JM, Kim SG, et al. 1992. Intrinsic signal changes accompanying sensory stimulation: functional brain mapping with magnetic resonance imaging. *PNAS* 89:5951–55

123. Thulborn KR, Waterton JC, Matthews PM, Radda GK. 1982. Oxygenation dependence of the transverse relaxation time of water protons in whole blood at high field. *Biochim. Biophys. Acta* 714:265–70
124. Attwell D, Buchan AM, Charpak S, Lauritzen M, MacVicar BA, Newman EA. 2010. Glial and neuronal control of brain blood flow. *Nature* 468:232–43
125. Fox PT, Raichle ME. 1986. Focal physiological uncoupling of cerebral blood flow and oxidative metabolism during somatosensory stimulation in human subjects. *PNAS* 83:1140–44
126. Petzold GC, Murthy VN. 2011. Role of astrocytes in neurovascular coupling. *Neuron* 71:782–97
127. Devor A, Dunn AK, Andermann ML, Ulbert I, Boas DA, Dale AM. 2003. Coupling of total hemoglobin concentration, oxygenation, and neural activity in rat somatosensory cortex. *Neuron* 39:353–59
128. Otsu Y, Couchman K, Lyons DG, Collot M, Agarwal A, et al. 2015. Calcium dynamics in astrocyte processes during neurovascular coupling. *Nat. Neurosci.* 18:210–18
129. Logothetis NK, Pauls J, Augath M, Trinath T, Oeltermann A. 2001. Neurophysiological investigation of the basis of the fMRI signal. *Nature* 412:150–57
130. Viswanathan A, Freeman RD. 2007. Neurometabolic coupling in cerebral cortex reflects synaptic more than spiking activity. *Nat. Neurosci.* 10:1308–12
131. Attwell D, Iadecola C. 2002. The neural basis of functional brain imaging signals. *Trends Neurosci.* 25:621–25
132. Logothetis NK, Wandell BA. 2004. Interpreting the BOLD signal. *Annu. Rev. Physiol.* 66:735–69
133. Thomsen K, Offenhauser N, Lauritzen M. 2004. Principal neuron spiking: neither necessary nor sufficient for cerebral blood flow in rat cerebellum. *J. Physiol.* 560:181–89
134. Rauch A, Rainer G, Logothetis NK. 2008. The effect of a serotonin-induced dissociation between spiking and perisynaptic activity on BOLD functional MRI. *PNAS* 105:6759–64
135. Goense JB, Logothetis NK. 2008. Neurophysiology of the BOLD fMRI signal in awake monkeys. *Curr. Biol.* 18:631–40
136. Shmuel A, Leopold DA. 2008. Neuronal correlates of spontaneous fluctuations in fMRI signals in monkey visual cortex: implications for functional connectivity at rest. *Hum. Brain Mapp.* 29:751–61
137. Schölvinck ML, Maier A, Frank QY, Duyn JH, Leopold DA. 2010. Neural basis of global resting-state fMRI activity. *PNAS* 107:10238–43
138. He BJ, Snyder AZ, Zempel JM, Smyth MD, Raichle ME. 2008. Electrophysiological correlates of the brain's intrinsic large-scale functional architecture. *PNAS* 105:16039–44
139. Wen H, Liu Z. 2016. Separating fractal and oscillatory components in the power spectrum of neurophysiological signal. *Brain Topogr.* 29:13–26
140. Laufs H. 2008. Endogenous brain oscillations and related networks detected by surface EEG-combined fMRI. *Hum. Brain Mapp.* 29:762–69
141. Nunez PL, Silberstein RB. 2000. On the relationship of synaptic activity to macroscopic measurements: Does co-registration of EEG with fMRI make sense? *Brain Topogr.* 13:79–96
142. Michel CM, Murray MM, Lantz G, Gonzalez S, Spinelli L, de Peralta RG. 2004. EEG source imaging. *Clin. Neurophysiol.* 115:2195–222
143. Leopold DA, Maier A. 2012. Ongoing physiological processes in the cerebral cortex. *NeuroImage* 62:2190–200
144. Liu Z, de Zwart JA, Chang C, Duan Q, van Gelderen P, Duyn JH. 2014. Neuroelectrical decomposition of spontaneous brain activity measured with functional magnetic resonance imaging. *Cereb. Cortex* 24:3080–89
145. Ritter P, Schirner M, McIntosh AR, Jirsa VK. 2013. The virtual brain integrates computational modeling and multimodal neuroimaging. *Brain Connect.* 3:121–45
146. Ahlfors SP, Simpson GV, Dale AM, Belliveau JW, Liu AK, et al. 1999. Spatiotemporal activity of a cortical network for processing visual motion revealed by MEG and fMRI. *J. Neurophysiol.* 82:2545–55
147. Bledowski C, Kadosh KC, Wibral M, Rahm B, Bittner RA, et al. 2006. Mental chronometry of working memory retrieval: a combined functional magnetic resonance imaging and event-related potentials approach. *J. Neurosci.* 26:821–29
148. Liu AK, Belliveau JW, Dale AM. 1998. Spatiotemporal imaging of human brain activity using functional MRI constrained magnetoencephalography data: Monte Carlo simulations. *PNAS* 95:8945–50

149. Dale AM, Liu AK, Fischl BR, Buckner RL, Belliveau JW, et al. 2000. Dynamic statistical parametric mapping: combining fMRI and MEG for high-resolution imaging of cortical activity. *Neuron* 26:55–67
150. Liu Z, He B. 2008. fMRI-EEG integrated cortical source imaging by use of time-variant spatial constraints. *NeuroImage* 39:1198–214
151. Liu Z, Rios C, Zhang N, Yang L, Chen W, He B. 2010. Linear and nonlinear relationships between visual stimuli, EEG and BOLD fMRI signals. *NeuroImage* 50:1054–66
152. Liu Z, Zhang N, Chen W, He B. 2009. Mapping the bilateral visual integration by EEG and fMRI. *NeuroImage* 46:989–97
153. Shmuel A, Augath M, Oeltermann A, Logothetis NK. 2006. Negative functional MRI response correlates with decreases in neuronal activity in monkey visual area V1. *Nat. Neurosci.* 9:569–77
154. Makeig S, Westerfield M, Jung T-P, Enghoff S, Townsend J, et al. 2002. Dynamic brain sources of visual evoked responses. *Science* 295:690–94
155. Raichle ME, Mintun MA. 2006. Brain work and brain imaging. *Annu. Rev. Neurosci.* 29:449–76
156. Sadaghiani S, Hesselmann G, Friston KJ, Kleinschmidt A. 2010. The relation of ongoing brain activity, evoked neural responses, and cognition. *Front. Syst. Neurosci.* 4:20
157. He B. 2013. Spontaneous and task-evoked brain activity negatively interact. *J. Neurosci.* 33:4672–82
158. Murta T, Leite M, Carmichael DW, Figueiredo P, Lemieux L. 2015. Electrophysiological correlates of the BOLD signal for EEG-informed fMRI. *Hum. Brain Mapp.* 36:391–414
159. Mantini D, Perrucci MG, Del Gratta C, Romani GL, Corbetta M. 2007. Electrophysiological signatures of resting state networks in the human brain. *PNAS* 104:13170–75
160. Buzsáki G, Draguhn A. 2004. Neuronal oscillations in cortical networks. *Science* 304:1926–29
161. Olbrich S, Mulert C, Karch S, Trenner M, Leicht G, et al. 2009. EEG-vigilance and BOLD effect during simultaneous EEG/fMRI measurement. *NeuroImage* 45:319–32
162. Leopold DA, Murayama Y, Logothetis NK. 2003. Very slow activity fluctuations in monkey visual cortex: implications for functional brain imaging. *Cereb. Cortex* 13:422–33
163. Ritter P, Moosmann M, Villringer A. 2009. Rolandic α and β EEG rhythms' strengths are inversely related to fMRI-BOLD signal in primary somatosensory and motor cortex. *Hum. Brain Mapp.* 30:1168–87
164. Liu Y, Bengson J, Huang H, Mangun GR, Ding M. 2014. Top-down modulation of neural activity in anticipatory visual attention: control mechanisms revealed by simultaneous EEG-fMRI. *Cereb. Cortex* 26:517–29
165. Laufs H, Kleinschmidt A, Beyerle A, Eger E, Salek-Haddadi A, et al. 2003. EEG-correlated fMRI of human α activity. *NeuroImage* 19:1463–76
166. Liu Z, de Zwart JA, Yao B, van Gelderen P, Kuo L-W, Duyn JH. 2012. Finding thalamic BOLD correlates to posterior α EEG. *NeuroImage* 63:1060–69
167. Scheeringa R, Bastiaansen MC, Petersson KM, Oostenveld R, Norris DG, Hagoort P. 2008. Frontal θ EEG activity correlates negatively with the default mode network in resting state. *Int. J. Psychophysiol.* 67:242–51
168. He BJ, Zempel JM, Snyder AZ, Raichle ME. 2010. The temporal structures and functional significance of scale-free brain activity. *Neuron* 66:353–69
169. Jensen O, Colgin LL. 2007. Cross-frequency coupling between neuronal oscillations. *Trends Cogn. Sci.* 11:267–69
170. Wen H, Liu Z. 2016. Broadband electrophysiological dynamics contribute to global resting-state fMRI signal. *J. Neurosci.* 36:6030–40
171. Scheeringa R, Fries P, Petersson K-M, Oostenveld R, Grothe I, et al. 2011. Neuronal dynamics underlying high-and low-frequency EEG oscillations contribute independently to the human BOLD signal. *Neuron* 69:572–83
172. Lehmann D, Michel CM. 2011. EEG-defined functional microstates as basic building blocks of mental processes. *Clin. Neurophysiol.* 122:1073–74
173. Musso F, Brinkmeyer J, Mobascher A, Warbrick T, Winterer G. 2010. Spontaneous brain activity and EEG microstates. A novel EEG/fMRI analysis approach to explore resting-state networks. *NeuroImage* 52:1149–61

174. Britz J, Van De Ville D, Michel CM. 2010. BOLD correlates of EEG topography reveal rapid resting-state network dynamics. *NeuroImage* 52:1162–70
175. Yuan H, Zotev V, Phillips R, Drevets WC, Bodurka J. 2012. Spatiotemporal dynamics of the brain at rest—exploring EEG microstates as electrophysiological signatures of BOLD resting state networks. *NeuroImage* 60:2062–72
176. Eichele T, Specht K, Moosmann M, Jongsma ML, Quiroga RQ, et al. 2005. Assessing the spatiotemporal evolution of neuronal activation with single-trial event-related potentials and functional MRI. *PNAS* 102:17798–803
177. Debener S, Ullsperger M, Siegel M, Engel AK. 2006. Single-trial EEG-fMRI reveals the dynamics of cognitive function. *Trends Cogn. Sci.* 10:558–63
178. Allen PJ, Josephs O, Turner R. 2000. A method for removing imaging artifact from continuous EEG recorded during functional MRI. *NeuroImage* 12:230–39
179. Neuner I, Arrubla J, Felder J, Shah NJ. 2014. Simultaneous EEG-fMRI acquisition at low, high and ultra-high magnetic fields up to 9.4 T: perspectives and challenges. *NeuroImage* 102:71–79
180. Liu Z, de Zwart JA, van Gelderen P, Kuo L-W, Duyn JH. 2012. Statistical feature extraction for artifact removal from concurrent fMRI-EEG recordings. *NeuroImage* 59:2073–87
181. Chowdhury ME, Mullinger KJ, Glover P, Bowtell R. 2014. Reference layer artefact subtraction (RLAS): a novel method of minimizing EEG artefacts during simultaneous fMRI. *NeuroImage* 84:307–19
182. Siegel M, Donner TH, Engel AK. 2012. Spectral fingerprints of large-scale neuronal interactions. *Nat. Rev. Neurosci.* 13:121
183. Hipp JF, Siegel M. 2015. BOLD fMRI correlation reflects frequency-specific neuronal correlation. *Curr. Biol.* 25:1368–74
184. Van Kerkoerle T, Self MW, Dagnino B, Gariel-Mathis M-A, Poort J, et al. 2014. α and γ oscillations characterize feedback and feedforward processing in monkey visual cortex. *PNAS* 111:14332–41
185. Bastos AM, Vezoli J, Bosman CA, Schoffelen J-M, Oostenveld R, et al. 2015. Visual areas exert feedforward and feedback influences through distinct frequency channels. *Neuron* 85:390–401
186. Michalareas G, Vezoli J, Van Pelt S, Schoffelen J-M, Kennedy H, Fries P. 2016. α-β and γ rhythms subserve feedback and feedforward influences among human visual cortical areas. *Neuron* 89:384–97
187. Scheeringa R, Koopmans PJ, van Mourik T, Jensen O, Norris DG. 2016. The relationship between oscillatory EEG activity and the laminar-specific BOLD signal. *PNAS* 113:6761–66
188. Klink PC, Dagnino B, Gariel-Mathis M-A, Roelfsema PR. 2017. Distinct feedforward and feedback effects of microstimulation in visual cortex reveal neural mechanisms of texture segregation. *Neuron* 95:209–20
189. Bastos AM, Usrey WM, Adams RA, Mangun GR, Fries P, Friston KJ. 2012. Canonical microcircuits for predictive coding. *Neuron* 76:695–711
190. Rao RP, Ballard DH. 1999. Predictive coding in the visual cortex: a functional interpretation of some extra-classical receptive-field effects. *Nat. Neurosci.* 2:79–87
191. Friston K. 2010. The free-energy principle: a unified brain theory? *Nat. Rev. Neurosci.* 11:127–38
192. Lang J. 2012. *Clinical Anatomy of the Head: Neurocranium Orbit Craniocervical Regions*. Berlin: Springer
193. Murphy M, Riedner BA, Huber R, Massimini M, Ferrarelli F, Tononi G. 2009. Source modeling sleep slow waves. *PNAS* 106:1608–13
194. Edelman BJ, Johnson N, Sohrabpour A, Tong S, Thakor N, He B. 2015. Systems neuroengineering: understanding and interacting with the brain. *Engineering* 1:292–308
195. Foxe JJ, Murray MM, Javitt DC. 2005. Filling-in in schizophrenia: a high-density electrical mapping and source-analysis investigation of illusory contour processing. *Cereb. Cortex* 15:1914–27
196. Zhang HC, Sohrabpour A, Lu Y, He B. 2016. Spectral and spatial changes of brain rhythmic activity in response to the sustained thermal pain stimulation. *Hum. Brain Mapp.* 37:2796–91
197. He B, Coleman T, Genin GM, Glover G, Hu X, et al. 2013. Grand challenges in mapping the human brain: NSF workshop report. *IEEE Trans. Biomed. Eng.* 60:2983–92
198. He B. 2016. Focused ultrasound help realize high spatiotemporal brain imaging? A concept on acousto-electrophysiological neuroimaging. *IEEE Trans. Biomed. Eng.* 63:2654–56
199. Oostenveld R, Fries P, Maris E, Schoffelen J-M. 2011. FieldTrip: open source software for advanced analysis of MEG, EEG, and invasive electrophysiological data. *Comput. Intell. Neurosci.* 2011:156869

200. Gramfort A, Luessi M, Larson E, Engemann DA, Strohmeier D, et al. 2014. MNE software for processing MEG and EEG data. *NeuroImage* 86:446–60
201. Dalal SS, Zumer JM, Agrawal V, Hild KE, Sekihara K, Nagarajan SS. 2004. NUTMEG: a neuromagnetic source reconstruction toolbox. *Neurol. Clin. Neurophysiol.* 2004:52
202. Tadel F, Baillet S, Mosher JC, Pantazis D, Leahy RM. 2011. Brainstorm: a user-friendly application for MEG/EEG analysis. *Comput. Intell. Neurosci.* 2011:879716
203. Delorme A, Makeig S. 2004. EEGLAB: an open source toolbox for analysis of single-trial EEG dynamics including independent component analysis. *J. Neurosci. Methods* 134:9–21
204. Brunet D, Murray MM, Michel CM. 2011. Spatiotemporal analysis of multichannel EEG: CARTOOL. *Comput. Intell. Neurosci.* 2011:813870
205. Penny WD, Friston KJ, Ashburner JT, Kiebel SJ, Nichols TE. 2011. *Statistical Parametric Mapping: The Analysis of Functional Brain Images*. San Diego: Academic
206. Ashburner J. 2012. SPM: a history. *NeuroImage* 62:791–800
207. Takahashi YD, Baccal AL, Sameshima K. 2007. Connectivity inference between neural structures via partial directed coherence. *J. Appl. Stat.* 34:1259–73
208. Delorme A, Mullen T, Kothe C, Acar ZA, Bigdely-Shamlo N, et al. 2011. EEGLAB, SIFT, NFT, BCILAB, and ERICA: new tools for advanced EEG processing. *Comput. Intell. Neurosci.* 2011:130714
209. Fischl B. 2012. FreeSurfer. *NeuroImage* 62:774–81
210. Shattuck DW, Leahy RM. 2002. BrainSuite: an automated cortical surface identification tool. *Med. Image Anal.* 6:129–42
211. Rivière D, Geffroy D, Denghien I, Souedet N, Cointepas Y. 2009. BrainVISA: an extensible software environment for sharing multimodal neuroimaging data and processing tools. *NeuroImage* 47:S163
212. Gramfort A, Papadopoulo T, Olivi E, Clerc M. 2010. OpenMEEG: opensource software for quasistatic bioelectromagnetics. *Biomed. Eng. Online* 9:45